Primary and secondary organic aerosol origin by combined gas-particle phase source apportionment

M. Crippa, F. Canonaco, J. G. Slowik, I. El Haddad, P. F. Decarlo, C. Mohr, M. F. Heringa, R. Chirico, Nicolas Marchand, B. Temime-Roussel, et al.

Atmos. Chem. Phys., 13, 8411–8426, 2013
www.atmos-chem-phys.net/13/8411/2013/
doi:10.5194/acp-13-8411-2013

Atmospheric Chemistry and Physics Open Access

Primary and secondary organic aerosol origin by combined gas-particle phase source apportionment

M. Crippa[1], F. Canonaco[1], J. G. Slowik[1], I. El Haddad[1], P. F. DeCarlo[1,*], C. Mohr[1,], M. F. Heringa[1,***], R. Chirico[1,****], N. Marchand[2], B. Temime-Roussel[2], E. Abidi[2], L. Poulain[3], A. Wiedensohler[3], U. Baltensperger[1], and A. S. H. Prévôt[1]**

[1]Laboratory of Atmospheric Chemistry, Paul Scherrer Institute, 5232 PSI Villigen, Switzerland
[2]Aix-Marseille Université, CNRS, LCE FRE 3416, 13331 Marseille, France
[3]Leibniz Institute for Tropospheric Research, Permoserstr 15, 04318 Leipzig, Germany
[*]now at: Department of Civil, Architectural, and Environmental Engineering and Department of Chemistry, Drexel University, Philadelphia, PA 19104, USA
[**]now at: Department of Atmospheric Sciences, University of Washington, Seattle, WA 98195, USA
[***]now at: WIL Research, 5203 DL's-Hertogenbosch, the Netherlands
[****]now at: Italian National Agency for New Technologies, Energy and Sustainable Economic Development (ENEA), UTAPRAD-DIM, Via E. Fermi 45, 00044 Frascati, Italy

Correspondence to: M. Crippa (monica.crippa@psi.ch)

Received: 8 February 2013 – Published in Atmos. Chem. Phys. Discuss.: 28 March 2013
Revised: 12 July 2013 – Accepted: 12 July 2013 – Published: 26 August 2013

Abstract. Secondary organic aerosol (SOA), a prominent fraction of particulate organic mass (OA), remains poorly constrained. Its formation involves several unknown precursors, formation and evolution pathways and multiple natural and anthropogenic sources. Here a combined gas-particle phase source apportionment is applied to wintertime and summertime data collected in the megacity of Paris in order to investigate SOA origin during both seasons. This was possible by combining the information provided by an aerosol mass spectrometer (AMS) and a proton transfer reaction mass spectrometer (PTR-MS). A better constrained apportionment of primary OA (POA) sources is also achieved using this methodology, making use of gas-phase tracers. These tracers made possible the discrimination between biogenic and continental/anthropogenic sources of SOA. We found that continental SOA was dominant during both seasons (24–50 % of total OA), while contributions from photochemistry-driven SOA (9 % of total OA) and marine emissions (13 % of total OA) were also observed during summertime. A semi-volatile nighttime component was also identified (up to 18 % of total OA during wintertime). This approach was successfully applied here and implemented in a new source apportionment toolkit.

1 Introduction

Organic compounds enter Earth's atmosphere through primary biogenic emissions from terrestrial and marine ecosystems and anthropogenic sources such as traffic and residential heating (Hallquist et al., 2009). They comprise an immensely complex mixture of gas (volatile organic compounds, VOCs) and particle (organic aerosol, OA) phase species in continuous evolution in the atmosphere through reversible phase partitioning, dry and wet deposition and chemical reactions with oxidant species such as OH (daytime) and NO_3 (nighttime) (Warneke et al., 2004). Such reactions are associated with the production of tropospheric ozone, oxygenated VOCs (e.g., formaldehyde, formic acid, acetone, etc., Vlasenko et al., 2009) and secondary organic aerosol (SOA), formed when VOC oxidation products have sufficiently low volatility to partition to the particle phase. A detailed understanding of the sources, transformations and fate of primary organic species and their oxidation products in the environment is crucial because of their central role played in human health, biogeochemical cycles and Earth's climate.

To describe the interaction between OA and VOCs, Robinson et al. (2007) combined laboratory and ambient studies, accounting both for the gas-particle partitioning of POA (since most primary emissions are semi-volatile, the amount of available POA depends on the gas-particle partitioning) and the gas phase oxidation of low-volatility vapors to produce SOA. Donahue et al. (2006) proposed the volatility basis set approach (VBS) which bins compounds according to their saturation vapor pressure (C^*) to describe their volatility evolution due to temperature and chemistry both in the gas and condensed phases. This VBS approach was further developed by the 2-D framework for OA aging (Jimenez et al., 2009; Donahue et al., 2011), which describes the evolution of organic compounds when they undergo oligomerization (producing less volatile compounds with similar O : C ratio), oxygenation reactions (leading to the formation of lower volatility compounds with higher O : C ratio due to functionalization) or fragmentation (producing higher volatility compounds with high O : C ratio) in the atmosphere. The relative importance of fragmentation versus functionalization was investigated by Donahue et al. (2012) and by Kroll et al. (2009).

In recent years, source apportionment of the organic fraction has been advanced by application of the positive matrix factorization (PMF) receptor model to aerosol mass spectrometer data (Lanz et al., 2007, 2010; Ng et al., 2010) and proton transfer reaction mass spectrometer (PTR-MS) measurements (Vlasenko et al., 2009; Yuan et al., 2012). Several studies (Zhang et al., 2007; Jimenez et al., 2009; Lanz et al., 2007, 2010; El Haddad et al., 2013) demonstrated the predominance of SOA relative to POA emitted from sources such as traffic (referred to as hydrocarbon-like OA, HOA) and wood burning (WBOA, although sometimes it is dominant) even in urban atmospheres (especially in Europe). These observations require higher SOA yields and production rates than those currently utilized by models. Major uncertainties include the sources and structure of the main SOA precursors and the processes by which they produce SOA (Hallquist et al., 2009). Several studies show the possibility to discriminate SOA components based on volatility, degree of oxygenation, etc. (e.g., semi-volatile and low-volatility oxygenated OA (SV-OOA and LV-OOA), Lanz et al., 2007; Heringa et al., 2012), but often no information about the emitting source (anthropogenic or biogenic) or the governing chemical/physical processes can be retrieved together with the characterization of the entire OA mass.

Here, an experimental OA/VOCs source apportionment approach is presented, adapting the methodology of Slowik et al. (2010), and applied to two measurement field campaigns performed in Paris in summer 2009 and winter 2010. The combination of organic particle measurements provided by the AMS (aerosol mass spectrometer) with co-located VOC measurements by a PTR-MS (proton transfer reaction mass spectrometer) allows (i) a more robust POA/SOA AMS classification, (ii) a better characterization of the secondary processes involving both organic phases, and (iii) identification of gaseous precursors for specific OA sources. Results from this experimental procedure are described and compared with previous PMF results applied to the AMS dataset only.

2 Methodologies

Two intensive measurement field campaigns were performed within the MEGAPOLI project (Megacities: Emissions, urban, regional and Global Atmospheric POLlution and climate effects, and Integrated tools for assessment and mitigation, http://megapoli.dmi.dk/index.html) in the Parisian area during summertime (1–31 July 2009) and wintertime (15 January–15 February 2010) (Beekmann et al., 2013). The measurements took place at an urban site in the core of the metropolitan area of Paris located in the garden and roof of the Le Laboratoire d'Hygiène de la Ville de Paris (LHVP, 48.83° latitude, 2.36° longitude, 55 m above sea level). A PM_{10} inlet was located at $\sim$ 6 m above ground level and a comprehensive suite of particle and gas-phase instrumentation was deployed at the site. Details about the instruments used at the LHVP site during the summer 2009 and winter 2010 campaigns can be found in Freutel et al. (2013) and Crippa et al. (2013a), respectively. Here we primarily discuss particle composition measurements from an Aerodyne aerosol mass spectrometer (AMS, Aerodyne, Billerica, USA) and VOC measurements from an Ionicon proton transfer reaction mass spectrometer (PTR-MS, Ionicon Analytik, Innsbruck, Austria).

Meteorological conditions were significantly different during the two campaigns. Marine air masses influenced the continent during the summer period, resulting in very low PM concentrations, while continental air masses strongly affected the air pollution in Paris during wintertime (especially in the middle and at the end of the campaign), enhancing aerosol concentrations.

2.1 Instrumentation

2.1.1 AMS

The AMS provides real time chemical composition and size distribution of PM_1 non-refractory species, defined as species that flash vaporize at 600 °C and 10^{-5} Torr. At LHVP, a high-resolution time-of-flight AMS (HR-ToF-AMS) was deployed during both campaigns. Details about this instrument can be found in DeCarlo et al. (2006). Briefly, aerosols are sampled through an aerodynamic lens, where they are focused into a narrow beam and accelerated to a velocity inversely related to their aerodynamic size. The particles are transmitted into a high vacuum detection chamber ($\sim 10^{-5}$ Torr), where they impact on a resistively-heated surface (600 °C) and vaporize. The resulting gas molecules are ionized by electron impact (EI, $\sim$ 70 eV) and analyzed by

time-of-flight mass spectrometry. The time resolution of the deployed AMS was 10 min; details regarding the sampling protocol, AMS data analysis, applied corrections (collection efficiency, relative ionization efficiencies, etc.) can be found elsewhere (Freutel et al., 2013; Crippa et al., 2013a). Here the organic mass spectral time series with unit mass resolution is used as input for the positive matrix factorization (PMF) source apportionment model (see Sect. 2.2), together with the corresponding time series of measurement uncertainties (Allan et al., 2003). For the purposes of PMF, the AMS uncertainty matrix accounts for electronic noise (which corresponds to a minimum random error in the number of ions detected during the sampling period), ion-to-ion variability at the detector and ion counting statistics, where the probability that a single molecule is ionized and detected is approximated as a Poisson distribution (Allan et al., 2003). In order to perform PMF, 268 AMS ions were considered (m/z range up to 300) and error pretreatment procedures were applied according to Ulbrich et al. (2009), as discussed below. Low signal-to-noise m/z values (SNR < 0.2) were removed, whereas "weak" variables ($0.2 <$ SNR < 2) were downweighted by a factor of 2. In the AMS data analysis procedure, certain organic peaks are not directly measured but rather calculated as a fraction of the organic signal at m/z 44 (Allan et al., 2004). The errors for these m/z were adjusted to prevent overweighting of the m/z 44 signal, following the method of Ulbrich et al. (2009); of these m/z 44-dependent peaks, m/z 19 and 20 were simply removed due to their negligible masses.

2.1.2 PTR-MS

A high sensitivity proton transfer reaction mass spectrometer (HS-PTR-MS) provided online measurements of the concentrations of volatile organic compounds with a time resolution of 2.5 min. Ionization occurs by the chemical reaction of H_3O^+ ions with gas phase species (R) having higher proton affinities than water (Eq. 1). The resulting ion (RH^+) is subsequently detected by a quadrupole mass spectrometer (Lindinger et al., 1998).

$$H_3O^+ + R \rightarrow RH^+ + H_2O \quad (1)$$

The proton transfer reaction is a soft ionization technique, which reduces fragmentation compared to, e.g., electron ionization used by the AMS (Lindinger et al., 1998; de Gouw and Warneke, 2007). Volume mixing ratios (VMR) are obtained from the difference between the ion count rate ($I_{cc=off}$) and the background signals ($I_{cc=on}$) in the system. Background measurements are performed using a catalytic converter heated to 350 °C, which efficiently removes VOCs from the inlet flow (de Gouw and Warneke, 2007):

$$VMR = \frac{1}{I_{H_3O^+} \cdot S} \cdot (I_{cc=off} - I_{cc=on}) \quad (2)$$

Therefore, the error associated with the VMR (ΔVMR) can be calculated as follows, assuming that the statistical error is the main source of error in $I_{cc=on}$ and $I_{cc=off}$ (de Gouw et al., 2003):

$$\Delta VMR = \frac{1}{I_{H_3O^+} \cdot S} \cdot \sqrt{\frac{I_{cc=off}}{\tau_{cc=off}} + \frac{I_{cc=on}}{\tau_{cc=on}}}, \quad (3)$$

where τ represents the dwell time with the catalyst on and off, $I_{H_3O^+}$ the count rate of H_3O^+ ions (in 10^6 counts s^{-1}) and S the species-dependent sensitivity needed to calculate PTR-MS concentrations based on theoretical prediction (de Gouw and Warneke, 2007). This value is used as the uncertainty input for source apportionment analysis.

In this work, the signals of 34 selected ions were monitored during both campaigns with dwell times ranging from 1 to 10 s. The PTR-MS was operated at standard conditions, i.e., using a 2.25 mbar ion drift pressure and a drift field intensity of 130 Td. These conditions limit clustering and VOC-water adduct formation. For the PMF analysis, ions affected by water clusters were removed (m/z 39 corresponding to $H_3O^+ \cdot H_2O$ and m/z 55 corresponding to $H_3O^+ \cdot (H_2O)_2$), as well as those contaminated by laboratory application of solvents (e.g., acetonitrile at m/z 42). A total 28 ions were included in the winter PMF analysis and 27 in the summer analysis (see Tables 1 and 2). During the campaigns, background measurements were performed every 4 days for 30 min and the resulting backgrounds were subtracted from the measurements prior to PMF analysis.

Differently from the AMS dataset treatment for PMF, no minimum error was applied to the PTRMS data since for all the variables the corresponding errors were bigger or comparable to three times the background variability.

Finally, note that quadrupole PTR-MS is capable only of unit mass resolution analysis, and that the assignment of each PTR-MS m/z to a specific ion (or parent compound) was therefore not always possible.

2.2 Positive matrix factorization on combined datasets

To perform a combined source apportionment of OA and VOCs, unified error and data matrices were created using the AMS and PTR-MS datasets. Data from both instruments were averaged to the same temporal resolution (10 min) and unified matrices containing data (or uncertainties) were obtained. Specifically, for the summer campaign the unified data matrix contained 268 AMS m/z, 27 PTR-MS m/z and 2391 time points (total dimensions: 295 data points $\times$ 2391 time points). For the winter campaign, the unified data matrix contained 268 AMS m/z, 28 PTR-MS m/z, and 4402 time points (total dimensions: 296 data points $\times$ 4402 time points). The uncertainty matrices had the same dimensions as their corresponding data matrices. The unified matrices were analyzed by PMF using the multi-linear engine (ME-2) algorithm (Paatero, 1999) to enable operation in the "robust"

Table 1. Relative source contribution to each PTR-MS m/z (winter campaign). Bold numbers refer to the sources with the highest contribution to each PTR-MS mass.

PTR-MS m/z	COA	WBOA	HOA	LV-OOA	SV-OOA$_{night}$	background
31	**21.7 %**	**21.1 %**	2.8 %	**20.1 %**	18.1 %	16.2 %
41	16.2 %	6.5 %	**27.8 %**	13.2 %	**26.3 %**	10.0 %
43	17.7 %	**23.1 %**	13.3 %	7.9 %	**21.5 %**	16.5 %
45	14.0 %	12.7 %	11.1 %	17.9 %	**29.8 %**	14.6 %
47	**27.9 %**	0.0 %	19.1 %	**24.3 %**	0.0 %	**28.7 %**
59	12.9 %	6.6 %	12.2 %	**32.4 %**	19.5 %	16.4 %
61	20.5 %	**35.7 %**	3.4 %	0.0 %	**26.0 %**	14.3 %
69	12.7 %	**34.0 %**	17.4 %	0.0 %	16.9 %	19.1 %
71	15.6 %	**25.9 %**	19.7 %	7.5 %	17.5 %	13.8 %
73	16.2 %	0.0 %	16.1 %	**28.5 %**	**27.6 %**	11.6 %
77	3.9 %	0.0 %	0.0 %	**50.8 %**	**36.4 %**	9.0 %
79	0.0 %	18.5 %	5.2 %	**46.1 %**	**20.8 %**	9.4 %
81	12.2 %	**27.3 %**	**27.6 %**	0.0 %	18.8 %	14.1 %
83	14.5 %	**34.4 %**	20.3 %	0.0 %	14.5 %	16.2 %
85	8.1 %	**43.5 %**	11.5 %	1.1 %	21.1 %	14.8 %
87	11.3 %	**41.3 %**	3.4 %	7.5 %	18.2 %	18.2 %
89	0.0 %	23.9 %	5.3 %	**31.9 %**	0.0 %	**38.8 %**
93	20.2 %	7.6 %	**41.9 %**	18.4 %	5.5 %	6.4 %
97	0.0 %	**52.5 %**	5.5 %	6.4 %	3.1 %	**32.5 %**
101	10.2 %	22.8 %	6.9 %	20.7 %	5.3 %	**34.2 %**
105	3.7 %	15.8 %	23.7 %	**26.1 %**	6.1 %	**24.6 %**
107	**25.0 %**	1.7 %	**39.7 %**	19.6 %	5.8 %	8.2 %
121	21.5 %	1.9 %	**38.0 %**	23.2 %	0.5 %	15.0 %
129	0.0 %	**34.2 %**	15.2 %	18.0 %	21.3 %	11.3 %
137	4.2 %	**35.5 %**	**32.1 %**	4.3 %	7.4 %	16.5 %
151	0.0 %	20.5 %	**29.8 %**	0.0 %	**43.1 %**	6.6 %
153	1.9 %	**42.0 %**	22.5 %	0.0 %	22.2 %	11.5 %

outlier treatment mode (in which outliers are dynamically downweighted) rather than the "pseudo-robust" technique used by Slowik et al. (2010) (in which the PMF algorithm is run in the "true" mode, outliers are identified and downweighted, and the algorithm is run again in the "true" mode with these adjusted uncertainties). No constraints were applied to the mass spectrum or time series. Configuration of ME-2 inputs and analysis of the results was performed in a new toolkit for Igor Pro (Wavemetrics, Inc., Portland, OR, USA) developed at the Paul Scherrer Institute (Canonaco et al., 2013).

Briefly, the PMF model describes the observation (in our case the AMS and PTR-MS measurements, x_{ij}) as a linear combination of a number of factors p (related to sources and/or processes during post-analysis) for each time step i and m/z j, whose contribution over time is always positive (g_{ij}) and whose mass spectra (f_{ij}) are static (see Eq. 4).

$$x_{ij} = \sum_{k=1}^{p} \left(g_{ik} \cdot f_{kj}\right) + e_{ij} \quad (4)$$

Here e_{ij} are the residuals, defined as the point-by-point difference between the input data and the model solution. The algorithm iteratively minimizes the quantity Q (see Eq. 5), which represents the sum of the squares of the uncertainty-scaled residuals across the entire dataset (Paatero and Tapper, 1994; Paatero, 1999):

$$Q = \sum_{i} \sum_{j} \left(e_{ij}/s_{ij}\right)^2. \quad (5)$$

Here s_{ij} denote the measurement uncertainties. When applying PMF to data acquired by a single instrument (e.g., AMS or PTR-MS), constant biases in error estimates marginally affect the apportionment, while when including data from several instruments these biases become problematic. Moreover, when combining two datasets to perform PMF, we must take into account that some instruments have stronger internal correlations within the dataset (e.g., the AMS tends to have characteristic patterns within a single mass spectrum due to the extensive fragmentation associated with the hard ionization (electron impact ionization)) and that some variables drive the apportionment more than others. Because of such issues, it can be the case that a PMF analysis using the uncertainties calculated for each instrument as described above produces a solution where one instrument is well-represented and the other poorly-represented, as indicated by analysis of the residuals. For this reason, we utilize

Table 2. Relative source contribution to each PTR-MS m/z (summer campaign). The average contribution of the two separated marine factors is reported here. Bold numbers refer to the sources with the highest contribution to each PTR-MS mass.

PTR-MS m/z	COA	HOA	SV-OOA$_{day}$	LV-OOA	SV-OOA$_{night}$	MOA
31	16.8 %	9.2 %	16.6 %	7.9 %	0.8 %	**24.4 %**
41	6.5 %	**35.2 %**	23.7 %	1.3 %	14.3 %	9.5 %
43	12.2 %	5.8 %	19.9 %	**24.6 %**	19.4 %	9.1 %
45	**34.1 %**	7.9 %	4.5 %	10.6 %	14.0 %	14.4 %
47	3.2 %	19.3 %	13.3 %	9.3 %	8.3 %	**23.3 %**
59	0.4 %	3.4 %	3.9 %	**34.7 %**	20.1 %	18.7 %
61	22.6 %	0.0 %	13.3 %	**26.1 %**	18.1 %	10.0 %
69	9.6 %	15.2 %	**54.1 %**	0.0 %	7.8 %	6.7 %
71	0.0 %	6.7 %	**72.2 %**	8.5 %	8.9 %	1.9 %
73	0.0 %	15.4 %	4.7 %	23.2 %	24.2 %	16.3 %
75	0.0 %	0.0 %	**39.1 %**	**35.0 %**	15.3 %	5.3 %
79	**32.3 %**	**53.4 %**	1.3 %	0.0 %	6.4 %	3.3 %
81	**26.9 %**	21.9 %	11.5 %	0.0 %	20.0 %	9.9 %
83	15.9 %	17.0 %	7.9 %	13.2 %	**28.6 %**	8.7 %
85	**34.9 %**	8.8 %	8.4 %	11.1 %	16.3 %	10.3 %
87	14.8 %	3.7 %	18.6 %	**21.7 %**	17.5 %	11.8 %
89	**29.8 %**	0.0 %	3.3 %	11.5 %	9.0 %	**23.2 %**
93	0.0 %	**61.9 %**	1.7 %	3.5 %	20.8 %	6.1 %
97	**37.6 %**	12.9 %	1.5 %	6.5 %	16.1 %	12.7 %
101	**31.2 %**	0.0 %	0.0 %	19.7 %	15.1 %	17.0 %
105	**33.4 %**	12.8 %	0.0 %	7.3 %	13.7 %	16.4 %
107	15.8 %	**43.4 %**	0.0 %	4.3 %	21.1 %	7.7 %
121	16.4 %	**34.7 %**	3.9 %	2.5 %	19.4 %	11.5 %
129	**41.6 %**	2.4 %	0.0 %	17.4 %	**24.1 %**	7.2 %
137	2.6 %	**30.4 %**	**24.1 %**	0.0 %	**25.8 %**	8.6 %
151	0.0 %	23.9 %	0.0 %	18.6 %	**45.0 %**	6.2 %
153	**27.7 %**	7.1 %	0.0 %	17.1 %	**32.7 %**	7.6 %

an instrument-dependent weighting procedure to ensure that both instruments are well-represented in the solution. This criterion is evaluated by comparing the mean of the absolute value of AMS and PTR-MS scaled residuals, denoted as $\overline{\Delta E}$ (Slowik et al., 2010), as discussed below in Eq. (8).

The scaling procedure is performed through the application of a scaling value (C_{PTR}) to the PTR-MS component of the error matrix to obtain new PTR-MS errors ($s_{ij,\mathrm{new}}$):

$$s_{ij,\mathrm{new}} = \frac{s_{ij}}{C_{\mathrm{PTR}}}. \quad (6)$$

An unweighted solution will correspond to $C_{\mathrm{PTR}} = 1$; C_{PTR} values greater than 1 decrease the PTR-MS errors and therefore more importance is given by the algorithm during the iteration to represent these data because they constitute a larger fraction of Q, while the opposite effect is produced by $C_{\mathrm{PTR}} < 1$. C_{PTR} scaling values were selected in the range 0.1–1 with a step of 0.1 and from 1 to 10 with a step of 1. The AMS components of the uncertainty matrix were left unchanged.

Outlier treatment is also needed when running PMF. Outliers are defined by Paatero and Hopke (2003) as data points for which the following relationship is satisfied: $| e_{ij}/s_{ij} | > \alpha$ (where α is user-defined and is typically set to 4). A "robust mode" was developed for PMF to minimize outlier effects (Paatero and Hopke, 2003). In this mode, outliers are dynamically downweighted at each step of the solution process according to

$$s_{ij,\mathrm{downweighted}} = h_{ij} s_{ij} = \sqrt{\left| \frac{e_{ij} s_{ij,\mathrm{new}}}{\alpha} \right|}, \quad (7)$$

where h_{ij} are the downweighting factors which are equal to 1 unless the outlier condition is satisfied. This outlier downweighting was applied dynamically within the ME-2 procedure, and thus represents a significant improvement over the protocol of Slowik et al. (2010), where static downweighting was applied externally.

Potentially satisfactory solutions, in which both instruments are well-represented, are identified using the $\overline{\Delta E}$ parameter, which compares the mean of the absolute value of scaled residual of the AMS and PTR-MS components of the unified dataset (see Eq. 8). $\overline{\Delta E}$ depends on both the scaling value C_{PTR} (see Fig. 1) and the number of factors in the solution. Both datasets are well represented by the model when $\overline{\Delta E}$ is close to zero; positive $\overline{\Delta E}$ represents an overweighting of the PTR-MS data while negative $\overline{\Delta E}$ represent

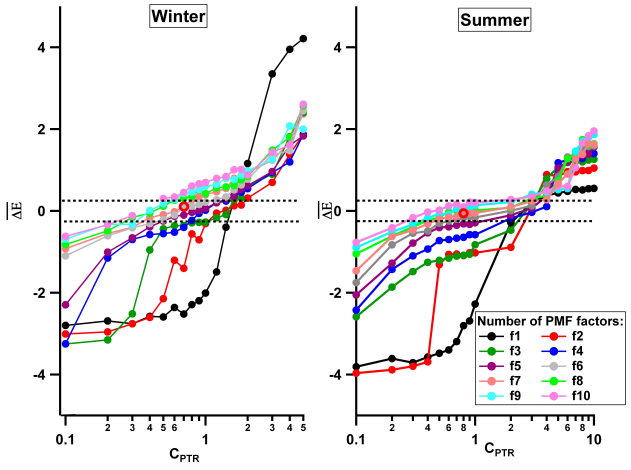

Fig. 1. $\overline{\Delta E}$ values as function of the number of PMF factors (colors) and C_{PTR} for the winter and summer campaigns. PMF solutions within the dashed lines (corresponding to 25 % deviation from $\overline{\Delta E}$ equal to zero) were analyzed in detail. The selected wintertime chosen solution has 6 factors and a C_{PTR} of 0.7, producing a $\overline{\Delta E}$ value of −0.025. The summertime solution has 7 factors and C_{PTR} of 0.8, producing a $\overline{\Delta E}$ value of −0.053. The chosen solutions are represented by the red circles.

an over-estimation of the AMS dataset. In the present study, we considered solutions with $-0.25 < \Delta E < 0.25$.

$$\overline{\Delta E} = \overline{\left(\frac{|e_{ij}|}{s_{ij}}\right)}_{\mathrm{AMS}} - \overline{\left(\frac{|e_{ij}|}{s_{ij}}\right)}_{\mathrm{PTRMS}} \quad (8)$$

Note that the object function Q, which is minimized during PMF execution, is calculated using the instrument-weighted errors with C_{PTR}, while $\overline{\Delta E}$ is evaluated considering the original errors. Selection of the "best" solution among those satisfying the $\overline{\Delta E}$ criterion is similar to conventional PMF analysis and is discussed further in Sect. 3.

2.3 Other data and source apportionment methods

Black carbon concentrations were measured using a 7-wavelength aethalometer measurement device (MAGEE Scientific, model AE31-ER). Levoglucosan and methanesulfonic acid were measured using $PM_{2.5}$ filters (quartz fiber filters, Tissuquartz®) analyzed by high-performance liquid chromatography with a mass spectrometric detector (Piot et al., 2012) and ion chromatography coupled with a conductivity detector, respectively.

In Sect. 3, results from the coupled PMF method discussed above are compared to other apportionment techniques, specifically (1) PMF of the AMS-only dataset (denoted as $\mathrm{PMF_{AMS}}$); (2) BC source apportionment based on the wavelength dependence of optical absorption; (3) tracer-based estimation of wood burning using levoglucosan; and (4) estimation of traffic POA emissions from BC measurements and reference OM/BC ratios. The PMF solutions of the PTR-MS-only dataset are not discussed here because we focus mainly on the quantification of sources contributing to the organic particle phase. Results from these methods have been presented in previous publications, as discussed below.

Method 1 ($\mathrm{PMF_{AMS}}$) provides the identification of OA primary and secondary sources. In our case, during wintertime, five sources were identified: hydrocarbon-like OA (HOA), cooking OA (COA) and wood burning OA (WBOA) as primary emissions, while the secondary fraction consists of oxygenated OA (OOA) and an oxygenated component mixed with WBOA ($\mathrm{OOA_2}$-BBOA) (Crippa et al., 2013a). In summertime, the $\mathrm{PMF_{AMS}}$ identified three components: COA, HOA and OOA (Freutel et al., 2013).

Method 2 (the aethalometer model) can be used to estimate the BC fraction emitted by different sources (e.g., traffic and wood burning, $\mathrm{BC_{tr}}$ and $\mathrm{BC_{wb}}$), based on the wavelength dependence of light absorption (Sandradewi et al., 2008; Healy et al., 2012), with the OM/BC ratios for primary traffic and wood burning estimated from the literature. For traffic the $\mathrm{OM/BC_{tr}}$ ratio was assumed to be 0.4 but it can vary from 0.2 up to 0.6 (Chirico et al., 2010; Favez et al., 2010). Wood burning conditions strongly affect the OM/BC and OM/levoglucosan ratios associated with this source. The OM/BC ratio for wood burning is reported to vary in smog chamber experiments between 1.6 and 3.5 (Grieshop et al., 2009; Heringa et al., 2011); however, much higher values are found in the ambient atmosphere (Favez et al., 2010; Sciare et al., 2011). A value of 15.1 was assumed here based on the measurements performed by Sciare et al. (2011) in the same region. The major source of BC was found to be traffic both during summer and winter, although during wintertime wood burning is also significant (∼ 20 %) (Crippa et al., 2013a).

The tracer-based methods 3 and 4 allow the estimation of the contribution of a specific source by using a molecular marker to define temporal behavior and scaling to the total source mass using an assumed source OA/marker ratio. However, the choice of representative emission ratios is quite variable since current literature values span a wide range. In our case the marker approach was used to estimate WBOA contribution from levoglucosan measurements and HOA mass from BC data. Here, the OM-to-levoglucosan ratio (∼ 12) measured by Sciare et al. (2011) for the Paris region was used, although studies in the literature report a wide range of variability for this ratio (OC/levoglucosan is reported to vary between 3–25 for chamber studies and 10–17 for ambient measurements) (Elsasser et al., 2012). Finally, in order to estimate the HOA contribution from the marker approach, the OM/BC ratio for traffic was assumed to be 0.4. The error bars reported in Figs. 4 and 7 refer to the variability range associated with the assumptions used for each apportionment method.

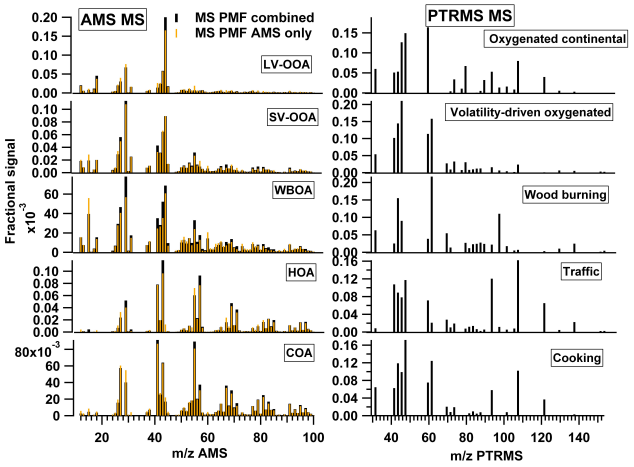

Fig. 2. Wintertime AMS and PTR-MS source mass spectra separated with the combined PMF approach. The spectra comparison with the PMF_{AMS} solution is also represented (Crippa et al., 2013a). Each mass spectrum is normalized to 1 both for the AMS and PTR-MS.

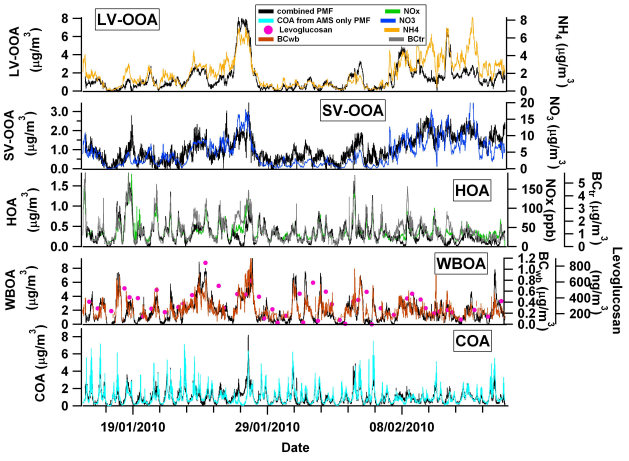

Fig. 3. Time series correlations between the retrieved PMF factors and external data (winter campaign). PMF factors concentrations refer only to the AMS fraction. The PTR-MS factors have the same temporal variation as the AMS ones but different absolute and relative concentrations.

3 Results

In this section PMF results retrieved from the combined $PMF_{AMS\text{-}PTRMS}$ for each season are presented individually, technically validated and compared with previous results obtained using PMF on AMS data only (PMF_{AMS}).

The solution was chosen based on several criteria: (i) selection of C_{PTR} values yielding near-zero $\overline{\Delta E}$ values (between -0.25 and $+0.25$) (Fig. 1), (ii) interpretation of mass spectra and comparison with reference spectra (Figs. 2 and 5), (iii) temporal correlation of the identified sources with complementary measurements (Figs. 3 and 6), and (iv) time series diurnal patterns (Sect. SI-2 of the Supplement).

First, based on the $\overline{\Delta E}$ criterion described in Sect. 2.2, a set of possible solutions was explored within the range $\overline{\Delta E} = 0 \pm 0.25$, considering from 1 to 10 factors. Solutions failing to satisfy this $\overline{\Delta E}$ criterion were discarded from further analysis. The effect of the instrument weighting procedure was also monitored for each solution through the residual diagnostic graphs (see also Sect. SI-4 of the Supplement). The remaining solutions were evaluated in terms of their physical meaning by analysis of diurnal variations, correlation with reference mass spectra and external time series as done in conventional PMF.

The coupled PMF solutions are discussed below, focusing on their differences from conventional AMS-only PMF. Also, a comparison of results obtained from the source apportionment techniques discussed in Sect. 2.3 is presented to evaluate the uncertainties in the different approaches. Since the main aim of this paper is to use the PTR-MS VOC data to improve the apportionment of particulate organic sources (OA), the nomenclature adopted for the retrieved $PMF_{AMS\text{-}PTRMS}$ OA sources will be used both when referring to the particulate and gaseous fractions. First, the winter case is explored, reporting results from the $PMF_{AMS\text{-}PTRMS}$ approach (Sect. 3.1.1) and the comparison with other source apportionment methods (Sect. 3.1.2). Then the summer case is discussed, both in terms of combined PMF results (Sect. 3.2.1) and comparison with other approaches (Sect. 3.2.2).

3.1 The winter case

3.1.1 Wintertime OA sources and VOC tracers

The chosen solution for the winter dataset consisted of six interpretable factors at a C_{PTR} value of 0.7, yielding $\Delta E = -0.025$ (Fig. 1). One of the factors consisted almost entirely of VOC species and was related to the PTR-MS background variability; this factor is therefore excluded from the following discussion of ambient factors (for additional information, see Sect. SI-5 of the Supplement). The other 5 factors were related to those obtained by PMF_{AMS} (Crippa et al., 2013a). However, the $PMF_{AMS\text{-}PTRMS}$ analysis provided improved separation of the primary and secondary factors compared to the PMF_{AMS} analysis. OA was here apportioned to three primary sources, including traffic (HOA), cooking (COA) and wood burning (WBOA), and two secondary fractions, including a low volatility (LV-OOA) and a semi-volatile (SV-OOA) oxygenated organic aerosol.

The AMS and PTR-MS factor mass spectra are shown in Fig. 2 and compared with those deconvolved by the PMF_{AMS} (Crippa et al., 2013a). Including VOCs measurements in PMF, some differences between the two apportionment techniques could be identified for the HOA concentrations (refer to Fig. SI-1.1 of the Supplement) due to the higher contribution of hydrocarbon peaks at m/z 43 and 57 to the

HOA mass spectrum from the combined PMF approach (see Fig. 2).

Figure 3 shows the correlation of the factor time series with external data, while the contribution of each factor to the total intensity of a PTR-MS m/z is shown in Table 1. Traffic, representing 6 % of total OA (see Fig. 8 below), dominates the gaseous alkane and alkene fragments (m/z 41, $C_3H_5^+$) and aromatics, such as benzene (m/z 79, $C_6H_6^+$), toluene (m/z 93, $C_7H_8^+$), C_8 aromatics and/or benzaldehyde (m/z 107, $C_7H_6O^+$ and/or $C_8H_{11}^+$), C_9 aromatics (m/z $C_9H_{13}^+$) and/or tolualdehyde (m/z 121, $C_8H_8O^+$ and/or $C_9H_{13}^+$), in agreement with studies in the literature (Jordan et al., 2009; Slowik et al., 2010). Additionally, Vlasenko et al. (2009) performed VOC source apportionment using PMF on a set of PTR-MS masses, identifying significant contributions at m/z 41, 43, 45, 57, 79, 93, 105, 107, 121, 135 for primary anthropogenic emissions, consistent with our observations.

Cooking emissions (18 % of OA mass) were characterized by a prominent diurnal pattern with increases during meal times (Fig. SI-2.1). The PMF_{AMS} and $PMF_{AMS\text{-}PTRMS}$ approach yielded similar results, meaning that the contribution of this source is not affected by any included gas phase tracer and that it was already clearly separated by PMF_{AMS}. Cooking has only recently been identified as an important source of primary OA (He et al., 2010; Sun et al., 2012; Mohr et al., 2012; Crippa et al., 2013a), and there is currently a need to identify atmospheric tracers for this source. Data on gas-phase emissions from cooking processes are very scarce, and therefore it is possible that optimal gas-phase cooking tracers occur at ions that were not selected for measurement by the PTR-MS. Previous measurements of VOCs from cooking identified mainly aldehydes and furan derivatives (Schauer et al., 2002). The PMF analyses indicate that cooking emissions only marginally impact the gas phase species selected for measurement. Of this subset, potential tracers include m/z 89, 97, 101, 129. Preliminary PTR-TOF-MS measurements of emissions from heated oils conducted in our laboratory (unpublished) suggest some of these m/z relate to furan derivatives (e.g., substituted furans at m/z 97, $C_6H_9O^+$) and alcohol and/or aldehyde fragments (e.g. $C_7H_{13}^+$ at m/z 97 and m/z 115 possibly corresponding to the dehydrated protonated ion $C_7H_{15}O^+$). The COA factor mass spectrum also includes peaks often associated with aromatic compounds, namely m/z 107 (C_8 aromatics) and 121 (C_9 aromatics). The presence of these species in cooking emissions is consistent with the findings of Slowik et al. (2010) and with our laboratory measurements. Possible explanations are (i) aromatics emitted from charbroiling-type meat cooking, (ii) contemporary emission and overlap between cooking and traffic sources due to geographical conditions, and (iii) mixture of HOA and COA due to meteorological conditions, transport and common back trajectories/wind direction. Further emission measurements are needed to identify gas phase tracers from cooking processes and characterize their true chemical nature. The lack of a dominant contribution from a particular VOC in Table 1 also indicates that the selected subset of PTR-MS masses does not contain a good cooking marker. Future high resolution PTR-MS measurements would indeed provide more resolved and comprehensive information on the gas-phase composition, which may aid the identification of specific cooking emission markers.

Concerning wood burning emissions (33 % of OA mass), a number of studies report acetonitrile (m/z 42, CH_3CN^+) and acetic acid (m/z 61, $C_2H_4O_2^+$) (Holzinger et al., 2005; Jordan et al., 2009) as important gas-phase wood burning tracers. However, in the present study m/z 42 was excluded from the PTR-MS dataset due to local contamination from the laboratory exhausts located on the roof of the LHVP building (acetonitrile was used in extraction systems and for a high performance liquid chromatography (HPLC) detection method). Other VOCs reported to have wood burning as a major source include formaldehyde, (m/z 31, CH_2O^+), methanol (m/z 33, CH_4O^+), acetaldehyde (m/z 45, $C_2H_4O^+$), and acetone (m/z 59, $(CH_3)_2CO^+$) (Holzinger et al., 1999, 2005; Schauer et al., 2001; Christian et al., 2003). In the present work, wood burning mainly contributed significantly to the following PTR-MS masses, consistent with the literature: m/z 61 (acetic acid, as found by Jordan et al., 2009); m/z 97 (furan derivatives, C_7 n-aldehydes fragment ion, as found by Schauer et al. (2001) and by Karl et al. (2007) with GC-PTRMS measurements); m/z 129 (naphthalene, $C_{10}H_9^+$); m/z 137 (monoterpenes, $C_{10}H_{17}^+$); m/z 153 ($C_8H_9O_3^+$, vanillin and isomers, as reported by Simoneit et al., 1999); m/z 69 (isoprene ($C_5H_9^+$) and furan ($C_4H_5O^+$)); m/z 71 (methacrolein ($C_4H_7O^+$) and/or methyl vinyl ketone (MVK, $C_4H_7O^+$), alkane and alkene fragments); m/z 85 (among possible candidates, ethyl vinyl ketone, alkanes and alkenes fragments, Akagi et al., 2011); and m/z 87 (among possible candidates, 2,3-butanedione, $C_4H_7O_2^+$, C-5 carbonyls, $C_5H_{11}O^+$).

For the winter case, two secondary OA sources were separated, namely the LV-OOA and SV-OOA. LV-OOA was identified as a major OA fraction, contributing 24 % to the total OA mass. Unsurprisingly, this fraction was found to dominate most of the oxygenated VOCs associated with long-range transported aged air masses, including, as possible candidates, formic acid (m/z 47, $CH_3O_2^+$), acetone (m/z 59, $C_3H_7O^+$), acetic acid (m/z 61, $C_2H_5O_2^+$), methyl ethyl ketone and methyl glyoxal (m/z 73, $C_4H_9O^+$ and $C_3H_5O_2^+$), in agreement with the literature (Vlasenko et al., 2009; Jordan et al., 2009; Slowik et al., 2010; Bon et al., 2011). Interestingly, during wintertime LV-OOA was significantly correlated with benzene (m/z 79), a tracer for anthropogenic emissions with a long lifetime ($R^2 = 0.47$), and with peroxyacetic nitric anhydride ($R^2 = 0.52$) (PAN, $CH_3C(O)OONO_2$, observed at m/z 77, corresponding to protonated peroxyacetic acid, $C_2H_5O_3^+$) produced by the oxidation of anthropogenic emissions under high NO_x; moreover, benzene

and PAN were also mainly apportioned to the secondary sources (see Table 1). While benzene and PAN are thought to be mainly associated with traffic emissions, benzene can also be emitted from wood burning, and certain PANs can form from fire emissions as well, as shown by Crounse et al. (2009) for Mexico City. These results suggest that the air masses associated with LV-OOA were influenced by continental/anthropogenic emissions, in agreement with previous findings for the Paris region, where air quality was found to be mainly affected by regional air masses (Beekmann et al., 2013). ^{14}C results revealed that the major fraction of OOA had a non-fossil origin (Beekmann et al., 2013), suggesting that biomass burning dominated the formation of this fraction compared to traffic. A possible explanation could be that the PTR-MS did not measure the relevant markers for biogenic oxidation products and therefore we cannot exclude the presence of oxidation products coming from other sources (e.g., biogenic emissions) within the same air masses.

Finally, the SV-OOA factor represented 18 % of the total OA mass and was defined based on the observation that this fraction peaks during nighttime, showing an anti-correlation with the temperature, similar to nitrate.

3.1.2 Comparison of source apportionment methods (winter)

Comparisons between factor contributions and time series obtained by $PMF_{AMS\text{-}PTRMS}$ and PMF_{AMS} are reported in Fig. 4 and Fig. SI-1.1 of the Supplement. As noted above, $PMF_{AMS\text{-}PTRMS}$ and PMF_{AMS} provided qualitatively similar factors; however, inclusion of VOC data in $PMF_{AMS\text{-}PTRMS}$ reduced mixing between factors and improved correlations with independently measured tracer species. Even though no significant differences were obtained in terms of OA mass spectra between the two approaches, factor time series and contributions showed significant discrepancies.

Major differences within the primary sources were obtained for the wood burning factor, where much higher contributions were observed for $PMF_{AMS\text{-}PTRMS}$. This increase was caused by a clearer separation between the semi-volatile OA (termed OOA_2-BBOA in Crippa et al., 2013a) and WBOA, which were partially mixed in the PMF_{AMS} solution because they both increased during the night (Fig. SI-2.1). Including gas phase species in the PMF enhanced the correlation of SV-OOA and WBOA with NO_3^- (e.g., $R^2 = 0.55$ for $PMF_{AMS\text{-}PTRMS}$ vs. $R^2 = 0.15$ for the PMF_{AMS}) and levoglucosan ($R^2 = 0.83$) (Fig. 3), respectively, suggesting that the $PMF_{AMS\text{-}PTRMS}$ solution is more accurate. Finally, good agreement between the two techniques was obtained for LV-OOA.

Figure 4 compares the $PMF_{AMS\text{-}PTRMS}$ and PMF_{AMS} with independent source apportionment approaches, including the aethalometer model and the tracer-based approaches. The comparison of all these techniques is crucial to estimate the uncertainties associated with source apportionment, especially when considering different datasets and algorithms. Within the primary sources, the estimation of the cooking contribution was quite consistent between methods (PMF_{AMS} vs. $PMF_{AMS\text{-}PTRMS}$), as discussed above. On the other hand, as traffic emits primary organic aerosols (HOA), black carbon and gaseous compounds (e.g., benzene, toluene, aromatics, etc.), different source apportionment techniques might be affected by the type of measurements used as input data. The HOA contribution provided by different apportionment methods varied between 0.29 and 0.69 $\mu g\,m^{-3}$; the biggest discrepancy is observed for the tracer-based estimate due to the variability in the assumption of the OM/BC_{tr} ratio. The comparison of WBOA contributions estimated using different methods clearly highlighted the uncertainties underlying the apportionment of this source: WBOA estimates spanned a wide range, between 0.87–4.8 $\mu g\,m^{-3}$ (representing from 15 to 83 % the total OA mass), depending on the apportionment technique considered. On one hand, PMF_{AMS} underestimates the WBOA contribution (0.87 $\mu g\,m^{-3}$) due to the mixture of SOA and wood burning sources (Crippa et al., 2013a). On the other hand, including the gas phase species clearly enhanced the deconvolution of WBOA and increased its contribution (1.94 $\mu g\,m^{-3}$), but WBOA estimated by $PMF_{AMS\text{-}PTRMS}$ remained lower than the estimates obtained using the marker and aethalometer approaches (3.82 and 4.8 $\mu g\,m^{-3}$, respectively). This is presumably because of an overestimation of the WBOA/levoglucosan and $WBOA/BC_{wb}$ ratios as represented by the error bars (note that the assumed OM/levoglucosan ratio represents already the lowest ratio for ambient measurements). Moreover, when comparing the WBOA contribution from different methods, it is necessary to consider that these models are based on different concepts and thus they are not directly comparable (e.g., the marker approach does not take into account chemical aging, while PMF does).

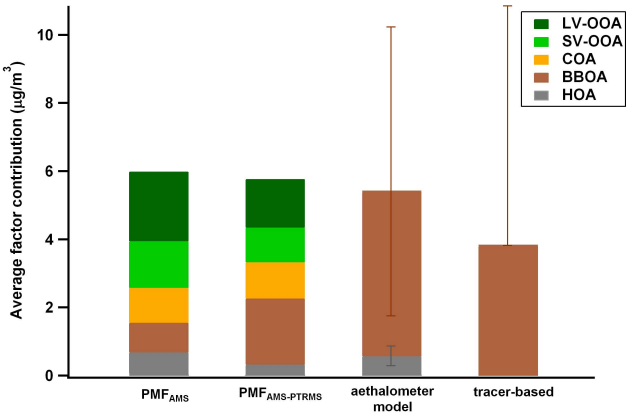

Fig. 4. Comparison of several source apportionment technique results in estimating OA sources during wintertime. Note that the aethalometer and marker approaches were attempted only for HOA and WBOA.

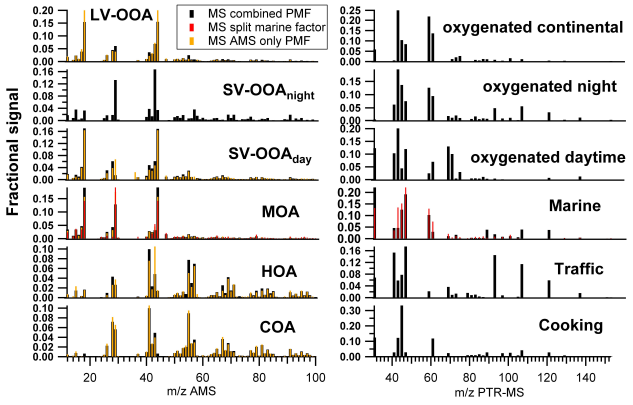

Fig. 5. Summertime AMS and PTR-MS source mass spectra separated with the combined PMF approach. The spectra comparison with the PMF$_{AMS}$ solution is also represented (Crippa et al., 2013b). In addition, in red the mass spectrum of the split marine factor from the 7-factor solution PMF is reported. Each mass spectrum is normalized to 1 both for the AMS and PTR-MS.

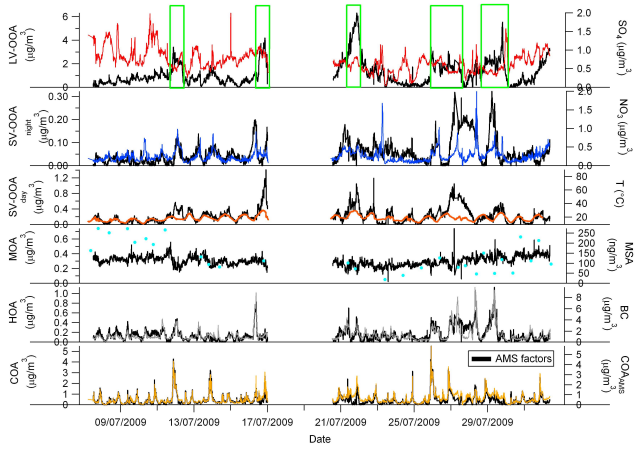

Fig. 6. Time series correlations between the retrieved PMF factors and external data (summer campaign). Green boxes delimit Atlantic polluted air masses identified with back trajectories, as reported by Freutel et al. (2013). PMF factors concentrations refer only to the AMS fraction. The PTR-MS factors have the same temporal variation as the AMS ones but different absolute and relative contributions.

Such an intercomparison exercise is very important; it highlights uncertainties related to the PMF$_{AMS}$ and marker based approaches. While differences between these apportionment techniques were previously observed, especially in winter (Favez et al., 2010), our results highlight the potential of the combined PMF$_{AMS\text{-}PTRMS}$ in improving source apportionment using PMF analysis. Meanwhile, there is a clear need for a better characterization of source emission profiles (marker to OA ratios) used in the apportionment.

3.2 The summer case

3.2.1 Summertime OA sources and VOC tracers

Combining the gas and particle phase datasets, we were able to distinguish seven factors. Two of them (HOA and COA) were identified as primary fractions. The others were related to secondary processes: LV-OOA (50 % of OA mass), nighttime SV-OOA (SV-OOA$_{night}$, 2 % of OA mass), photochemistry-driven SV-OOA (SV-OOA$_{day}$, 9 % of OA mass) and marine OA (MOA, 13 % of OA mass). The PMF solution returned two marine factors, which were combined into a single factor. The MOA time series was calculated as the sum of the time series contributions of the corresponding factors, and the aggregate mass spectrum was calculated as the mass-weighted average of the corresponding MS. Figure 1 shows the range of explored solutions as a function of the weighting parameter C_{PTR}. The chosen solution corresponds to a C_{PTR} value of 0.8, providing a $\Delta E = -0.053$. Figures 5 and 6 show the AMS and PTR-MS factor mass spectra and time series, respectively.

Traffic and cooking were identified as primary OA sources during summertime. The traffic factor mass spectrum is similar in summer and winter, as shown in Fig. SI-3.1 (see also Sect. 3.1.1). Likewise, the summer PTR-MS cooking spectrum (see Table 2) shows non-negligible contributions from aromatics and acetaldehyde, consistent with the winter case and the findings of Slowik et al. (2010), although as discussed above cooking activities are unlikely to constitute a major aromatic source. Further emission measurements are needed to characterize and quantify the contribution of gaseous emissions from cooking activities.

Concerning the secondary OA fractions, four components were separated during summertime (LV-OOA, SV-OOA$_{night}$, SV-OOA$_{day}$ and MOA), although during some events these SOA components showed a similar trend due to the role played by meteorology. As depicted in Fig. 6, during Atlantic polluted periods both the secondary sources and the HOA factor showed an increased mass concentration, meaning that during these events all factors were partially enhanced due to the contribution of polluted air masses. Similar to the winter case, LV-OOA represents the major OA fraction (50 %) and is mostly dominated by oxygenated VOCs (see Sect. 3.1.1 and Table 2). No insights about the anthropogenic or biogenic origin of this fraction were retrieved due to the lack of PTR-MS measurements of oxidation products of anthropogenic and biogenic emissions. The LV-OOA factor does not correlate well with SO_4, which is typically adopted as tracer for regional OA because of the occurrence of different types of air masses (continental, Atlantic clean and Atlantic polluted) and sources (refer to Freutel et al. (2013) for the air masses classification). Consequently, the LV-OOA diurnal pattern (see Fig. SI-2.2) is very different from the one of sulfate, probably also due to some contributions of primary

sources to this factor peaking during the evening hours, as highlighted by its diurnal pattern (e.g., from cooking).

SV-OOA$_{night}$ peaks at night and shows an anti-correlation with temperature, similar to nitrate. SV-OOA$_{night}$ contributes very little (2 %) to the total OA mass in summer. However, it has major contributions to some of the VOCs. Comparing the SV-OOA MS obtained for the winter case with the SV-OOA$_{night}$ MS from summer, the m/z 44 to m/z 43 ratio of this fraction varies substantially between summer and winter (0.20 and 1.39, respectively), suggesting different features between the 2 seasons. During summertime this SV-OOA fraction appears to be much more volatile than during wintertime, which could also explain its lower contribution in summer to total OA and the greater presence in the gas phase. During summertime the main VOC fragments contributing to this factor include (see Table 2) m/z 83, 129, 137, 151 and 153. Nighttime peaks of monoterpenes (m/z 137) and their first generation products such as pinonaldehyde (m/z 151) were often observed in previous studies and were related to enhanced nighttime emissions during the warm season and reduced oxidation due to low OH levels (Talbot et al., 2005; Jordan et al., 2009).

From the comparison of summertime and wintertime SV-OOA, different gaseous tracers were identified, which suggests different governing processes. As discussed above, during summer this factor has a strong biogenic component. For winter, m/z 151 remains an important peak, but signals at m/z 41, 43, 45, 61, 73, 77, 79 suggest a possible anthropogenic origin.

SV-OOA$_{day}$ exhibited a correlation with ambient temperature. Additional correlations with isoprene and its oxidation products suggest that this factor arises in large part from locally-formed biogenic SOA (although isoprene may be also emitted by anthropogenic sources such as oil and wood combustion, gasoline, tobacco etc., Adam et al., 2006). Isoprene (m/z 69), MVK/methacrolein (m/z 71) and monoterpenes (m/z 137) were the characteristic VOCs of this factor, in agreement with results reported by Jordan et al. (2009). Isoprene and monoterpenes are in fact emitted by plants during daytime and with increasing temperatures, while MVK and methacrolein are the major isoprene oxidation products. These results are in agreement with ^{14}C measurements performed during the MEGAPOLI summer campaign, which show summertime SOA being primarily non-fossil (80 %) (Beekmann et al., 2013).

Finally, marine organic aerosol was found to contribute 13 % to the total OA mass during the summer campaign, possibly due to high biological activity of the ocean in this season and the occurrence of oceanic air masses impacting the continent. Interestingly, marine emissions seem to dominate several secondary VOCs, including formaldehyde (m/z 31) and formic acid (m/z 47) in summer. Vlasenko et al. (2010) observed formaldehyde sensitivity being affected by humidity effects; however, we did not find an indication of overestimation due to a correlation with RH or water clusters (m/z 39 and 55) measured by the PTR-MS.

3.2.2 Comparison of source apportionment methods (summer)

Similarly to the winter case, results are here compared to several AMS-PMF estimates previously proposed for the same campaign (Fig. 7). Freutel et al. (2013) proposed a three-factor solution consisting of OOA, HOA and COA, based on unit mass resolution (UMR) PMF analysis. PMF analysis of high resolution AMS data for the same campaign at another site in Paris (SIRTA, Paris urban background) (Crippa et al., 2013b) yielded a five-factor solution: COA, HOA, continental LV-OOA, continental SV-OOA, and a marine factor (MOA) associated with oceanic air masses. Because aerosol composition was shown to be remarkably similar throughout the Paris region (Beekmann et al., 2013), it is reasonable to compare these results to the apportionment obtained in the present work. Since no additional sources could be clearly separated by the UMR PMF applied to the AMS data only, for comparison, the three- (COA, HOA and OOA) and the five- (COA, HOA, MOA, SV-OOA, LV-OOA) factors UMR PMF$_{AMS}$ solutions for the LHVP site are presented here.

Figure SI-1.2 shows good agreement between the PMF$_{AMS}$ and PMF$_{AMS\text{-}PTRMS}$ solutions for the two primary components HOA and COA and for LV-OOA, identified on the basis of their OA mass spectra (Fig. 5), diurnal cycles (reflecting the boundary layer evolution and the peak emission hours, Fig. SI-2.2) and correlation with external data (Fig. 6).

MOA, previously identified by Crippa et al. (2013b) due to its high correlation with MSA (methanesulfonic acid) and the predominance of sulfur containing fragments in its high resolution MS, is less well separated in PMF$_{AMS\text{-}PTRMS}$ without the high resolution information, as shown by the reduced correlation between MOA$_{AMS\text{-}PTRMS}$ and MSA (Fig. 6). Presumably this separation could be improved if high-resolution AMS data was available for incorporation into PMF$_{AMS\text{-}PTRMS}$.

A local semi-volatile OOA (SV-OOA) was previously identified by the PMF-AMS analysis (Crippa et al., 2013b). However, this factor appeared to be the product of two different processes: a temperature-driven partitioning and a production during peak photochemistry. By adding the gas phase species into the PMF$_{AMS\text{-}PTRMS}$ analysis, these processes were decoupled, yielding two SV-OOA factors: SV-OOA$_{day}$ and SV-OOA$_{night}$. On average, SV-OOA$_{day}$ mass builds steadily during the day, despite the development of the boundary layer, and significantly correlates with ozone and methacrolein + methyl vinyl ketone (m/z 71), short-lived early generation products of isoprene oxidation. This factor can be interpreted as stemming from the production of short-lived secondary organic compounds during peak photochemistry. By contrast, SV-OOA$_{night}$ contribution is enhanced during nighttime with the temperature decrease and the increase

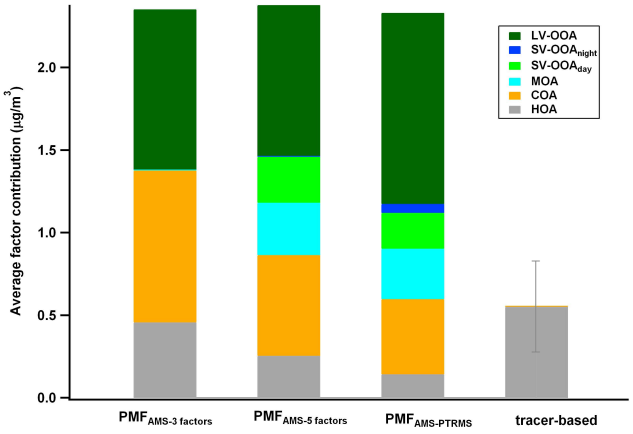

Fig. 7. Comparison of several source apportionment technique results in estimating OA sources during summertime. Note that the tracer-based approach was attempted only for HOA.

of relative humidity. This suggests that, similar to nitrate, this factor may be related to the partitioning of semi-volatile SOA into the particle phase.

Figure 7 presents the comparison of the different source apportionment results obtained by PMF$_{AMS\text{-}PTRMS}$ (six sources, present study), UMR PMF$_{AMS}$ (three factors, Freutel et al., 2013) and high resolution PMF$_{AMS}$ suggested for the SIRTA site (five factors, Crippa et al., 2013b). For HOA, a marker-based approach is also presented using BC as a specific tracer in absence of other combustion sources (see method 4 presented in Sect. 2.3). The three-factor solution shows higher contributions for COA, HOA and LV-OOA compared to the other cases, as they encompass the contributions of the other oxygenated components. When comparing the high resolution PMF$_{AMS}$ and the PMF$_{AMS\text{-}PTRMS}$ for the primary sources, ∼25 % and 47 % difference can be observed (COA and HOA, respectively). Better agreement between the two techniques is obtained for the secondary components: LV-OOA, MOA, SV-OOA represent 0.92–1.16, 0.31–0.32 and 0.22–0.28 µg m^{-3}, respectively (the latter considering the sum of SV-OOA$_{day}$ and SV-OOA$_{night}$ for the PMF$_{AMS\text{-}PTRMS}$).

4 Discussion and conclusions

Positive matrix factorization of aerosol mass spectra is a useful tool for identification of the contribution of both primary and secondary organic components (Zhang et al., 2011). However, for the secondary fraction, AMS-only PMF analysis typically reports OA only in terms of SV-OOA and LV-OOA fractions, which are distinguished mainly by volatility and degree of oxygenation but are difficult to further interpret. In this study a detailed investigation of organic aerosol sources was performed using positive matrix factorization applied to the combined AMS-PTRMS dataset during summertime and wintertime in Paris. This technique, implemented and tested within a new toolkit (Canonaco et al., 2013), was shown to be a useful and nonconventional approach within source apportionment methods. This approach was based on the treatment of data measured by several instruments and a weighting procedure in order to assure an equal model description of the observation over all instruments (in our case two).

However, a combined gas-particle phase source apportionment is a critical technique since it involves species with different lifetimes and several dynamic processes. This approach is suitable for a clearer identification of primary sources, where particulate and gaseous pollutants are co-emitted. On the other hand, secondary gas and particle phase species form and decay at different timescales; hence their covariance does not allow discrimination between different secondary sources, but instead may be used to infer the formation timescales and lifetimes of OOA species. A precursor concentration can be low because there is little emission of it or because it has high reactivity. In the first case the condensed species would be low, while in the second case the condensed species would be high. Such methodology has been successfully used in several works (Slowik et al., 2010; El Haddad et al., 2013), which have given valuable insights into the formation and aging processes of OOA.

Finally, a cleaner separation of primary sources by using a combined gas-particle phase source apportionment also allows a better separation of secondary sources (as demonstrated in our work for the winter case where the SV-OOA component is completely separated from the BBOA one differently from the PMF$_{AMS}$).

In our study, this technique provided insights on the secondary organic aerosol components, compared with previous studies performed on the same dataset. In fact, the combination of contemporary particle and gas phase measurements emitted by the same sources allowed a clearer discrimination of both primary and secondary OA, the identification of their natural or anthropogenic/continental origin and gaseous tracers. Specifically, SOA constituted more than 50 % of the OA mass in the Paris area and was classified in terms of continental, photochemistry-driven, volatility/nighttime-driven and marine components (though the continental vs. marine split is also possible through high-resolution analysis of AMS-only mass spectra).

Figure 8 shows the average contribution of primary and secondary sources for the total organic AMS measurements and the PTR-MS gas phase fraction. Primary OA sources (COA and HOA) did not present any seasonal variation due to their local origin and season-independent source activity. The traffic source contributed on average 6 % to the total OA mass during both campaigns, while cooking emissions represented on average 18–20 % of the total OA mass. Wood burning was also a significant wintertime source in Paris, contributing on average 33 % to the total OA mass.

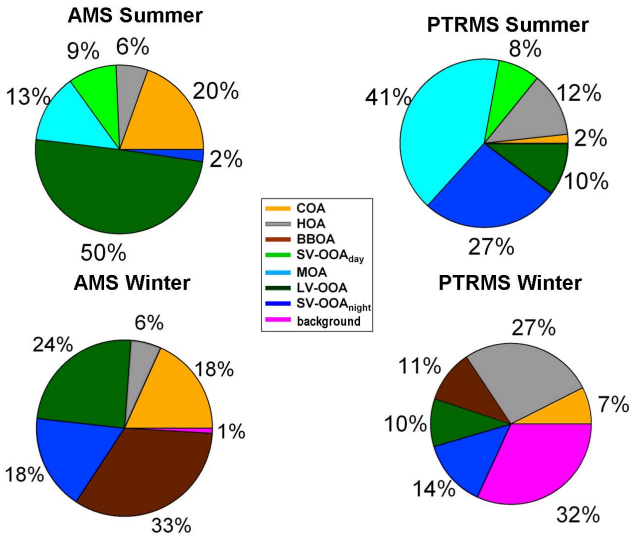

Fig. 8. Average AMS and PTR-MS source contributions for the summer and winter campaigns. The AMS relative contributions refer to the total organic aerosol mass, while the PTR-MS contributions refer to the total measured gas phase.

SOA constituted the major fraction of OA for both seasons (Freutel et al., 2013; Crippa et al., 2013a) and it was mainly formed from continental emissions oxidation and associated with the occurrence of aged air masses (especially during wintertime), contributing in winter 24 % and in summer 50 % to the total OA mass.

Continental SOA was previously classified by PMF_{AMS} according to degree of oxygenation and volatility as local semi-volatile OOA (SV-OOA) and regional aged OOA (LV-OOA), but without source-specific information on the precursors of these fractions. Beekmann et al. (2013) confirmed the regional behavior of OA sources, but did not relate the regional aged OA to specific time-of-day related processes. This is the new feature of the analysis in this paper. Another regional SOA factor derived from marine air masses could be observed only during summertime due to particular air mass regimes, contributing 13 % to the total OA mass, coherently with Crippa et al. (2013b).

With our work, we demonstrated the possibility to separate the SV-OOA source into a daytime and nighttime fraction by joining the gas and particle phase information provided by the PTR-MS and AMS data. A secondary nighttime component correlating with nitrate was separated, representing only 2 % of total OA during summer and 18 % in winter.

A smaller fraction of SOA was indeed produced locally, both during daytime (9 %) and nighttime (2 %) in summer. Daytime SOA was mainly produced by photochemistry, as confirmed by the correlation with isoprene, MVK, monoterpenes, temperature and solar radiation. Concerning the nighttime SOA, it was mainly associated with lower temperatures and it most probably implied nighttime chemistry involving monoterpenes and nitrates, etc. Finally, a cleaner SV-OOA factor was also separated during the winter measurements compared with the PMF_{AMS} solution where an oxygenated factor containing wood burning features was identified (OOA_2-BBOA).

As already mentioned, ^{14}C results showed that the major fraction of secondary OA had non-fossil origin during summertime (80 %) and wintertime (90 %) in Paris (Beekmann et al., 2013). Within the uncertainties associated with ^{14}C and other source apportionment methods, our summer results seem to be coherent with the ^{14}C findings due to the identification of a photochemistry driven and marine SOA sources in addition to a continental fraction, which might also be partially related to non-fossil origin.

Finally, concerning the winter solution, the presence of benzene and PAN in our LV-OOA factor suggests that this secondary fraction of OA could come from or form from biomass smoke in aged air masses, or that aged continental air masses influenced by anthropogenic emissions from traffic and biomass burning impacted the site, bringing benzene and PANs (from traffic) and LV-OOA (biomass burning SOA), coherently with ^{14}C data.

Supplementary material related to this article is available online at: http://www.atmos-chem-phys.net/13/8411/2013/acp-13-8411-2013-supplement.pdf.

Acknowledgements. This research, which was conducted in the context of the MEGAPOLI project, is mainly financially supported by the European Community's Framework Program FP/2007-2011 under grant agreement no. 212520, as well as the Swiss National Science Foundation and the French ANR project MEGAPOLI – PARIS under the grant agreement ANR-09-BLAN-0356. P. F. DeCarlo is grateful for postdoctoral fellowship support from a NSF International Postdoctoral Fellowship (0701013).

Edited by: A. Baklanov

References

Adam, T., Mitschke, S., Streibel, T., Baker, R. R., and Zimmermann, R.: Quantitative puff-by-puff-resolved characterization of selected toxic compounds in cigarette mainstream smoke, Chem. Res. Toxicol., 19, 511–520, 2006.

Akagi, S. K., Yokelson, R. J., Wiedinmyer, C., Alvarado, M. J., Reid, J. S., Karl, T., Crounse, J. D., and Wennberg, P. O.: Emission factors for open and domestic biomass burning for use in atmospheric models, Atmos. Chem. Phys., 11, 4039–4072, doi:10.5194/acp-11-4039-2011, 2011.

Allan, J. D., Jimenez, J. L., Williams, P. I., Alfarra, M. R., Bower, K. N., Jayne, J. T., Coe, H., and Worsnop, D. R.: Quantitative sampling using an Aerodyne aerosol mass spectrometer 1. Techniques of data interpretation and error analysis, J. Geophys. Res., 108, 4090, doi:10.1029/2002JD002358, 2003.

Allan, J. D., Delia, A. E., Coe, H., Bower, K. N., Alfarra, M. R., Jimenez, J. L., Middlebrook, A. M., Drewnick, F., Onasch, T. B., Canagaratna, M. R., Jayne, J. T., and Worsnop, D. R.: A generalised method for the extraction of chemically resolved mass spectra from Aerodyne aerosol mass spectrometer data, J. Aerosol Sci., 35, 909–922, 2004.

Beekmann, M., Prevot, A. S. H., Drewnick, F., Sciare, J., Pandis, S. N., Denier van der Gon, H. A. C., Crippa, M., Freutel, F., Poulain, L., Ghersi, V., Rodriguez, E., Beirle, S., Zotter, P., von der Weiden-Reinmüller, S.-L., Bressi, M., Fountoukis, C., Petetin, H., Szidat, S., Schneider, J., Rosso, A., El Haddad, I., Megaritis, A., Zhang, Q. J., Slowik, J. G., Moukhtar, S., Kolmonen, P., Stohl, A., Eckhardt, S., Borbon, A., Gros, V., Marchand, N., Jaffrezo, J. L., Schwarzenboeck, A., Colomb, A., Wiedensohler, A., Borrmann, S., Lawrence, M., Baklanov, A., and Baltensperger, U.: Regional emissions control fine particulate matter levels in the Paris Megacity, P. Natl. Acad. Sci., in preparation, 2013.

Bon, D. M., Ulbrich, I. M., de Gouw, J. A., Warneke, C., Kuster, W. C., Alexander, M. L., Baker, A., Beyersdorf, A. J., Blake, D., Fall, R., Jimenez, J. L., Herndon, S. C., Huey, L. G., Knighton, W. B., Ortega, J., Springston, S., and Vargas, O.: Measurements of volatile organic compounds at a suburban ground site (T1) in Mexico City during the MILAGRO 2006 campaign: measurement comparison, emission ratios, and source attribution, Atmos. Chem. Phys., 11, 2399–2421, doi:10.5194/acp-11-2399-2011, 2011.

Canonaco, F., Crippa, M., Slowik, J. G., Baltensperger, U., and Prévôt, A. S. H.: SoFi, an Igor based interface for the efficient use of the generalized multilinear engine (ME-2) for source apportionment: application to aerosol mass spectrometer data, Atmos. Meas. Tech. Discuss., 6, 6409–6443, doi:10.5194/amtd-6-6409-2013, 2013.

Chirico, R., DeCarlo, P. F., Heringa, M. F., Tritscher, T., Richter, R., Prévôt, A. S. H., Dommen, J., Weingartner, E., Wehrle, G., Gysel, M., Laborde, M., and Baltensperger, U.: Impact of aftertreatment devices on primary emissions and secondary organic aerosol formation potential from in-use diesel vehicles: results from smog chamber experiments, Atmos. Chem. Phys., 10, 11545–11563, doi:10.5194/acp-10-11545-2010, 2010.

Christian, T. J., Kleiss, B., Yokelson, R. J., Holzinger, R., Crutzen, P. J., Hao, W. M., Saharjo, B. H., and Ward, D. E.: Comprehensive laboratory measurements of biomass-burning emissions: 1. Emissions from Indonesian, African, and other fuels, J. Geophys. Res.-Atmos., 108, 4719, doi:10.1029/2003JD003704, 2003.

Crippa, M., DeCarlo, P. F., Slowik, J. G., Mohr, C., Heringa, M. F., Chirico, R., Poulain, L., Freutel, F., Sciare, J., Cozic, J., Di Marco, C. F., Elsasser, M., Nicolas, J. B., Marchand, N., Abidi, E., Wiedensohler, A., Drewnick, F., Schneider, J., Borrmann, S., Nemitz, E., Zimmermann, R., Jaffrezo, J.-L., Prévôt, A. S. H., and Baltensperger, U.: Wintertime aerosol chemical composition and source apportionment of the organic fraction in the metropolitan area of Paris, Atmos. Chem. Phys., 13, 961–981, doi:10.5194/acp-13-961-2013, 2013a.

Crippa, M., El Haddad, I., Slowik, J. G., DeCarlo, P. F., Mohr, C., Heringa, M., Chirico, R., Marchand, N., Sciare, J., Baltensperger, U., and Prévôt, A. S. H.: Identification of marine and continental aerosol sources in Paris using high resolution aerosol mass spectrometry, J. Geophys. Res., 118, 1950–1963, doi:10.1002/jgrd.50151, 2013b.

Crounse, J. D., DeCarlo, P. F., Blake, D. R., Emmons, L. K., Campos, T. L., Apel, E. C., Clarke, A. D., Weinheimer, A. J., McCabe, D. C., Yokelson, R. J., Jimenez, J. L., and Wennberg, P. O.: Biomass burning and urban air pollution over the Central Mexican Plateau, Atmos. Chem. Phys., 9, 4929–4944, doi:10.5194/acp-9-4929-2009, 2009.

de Gouw, J. and Warneke, C.: Measurements of volatile organic compounds in the earth's atmosphere using proton-transfer-reaction mass spectrometry, Mass Spectrom. Rev., 26, 223–257, 2007.

de Gouw, J. A., Goldan, P. D., Warneke, C., Kuster, W. C., Roberts, J. M., Marchewka, M., Bertman, S. B., Pszenny, A. A. P., and Keene, W. C.: Validation of proton transfer reaction-mass spectrometry (PTR-MS) measurements of gas-phase organic compounds in the atmosphere during the New England Air Quality Study (NEAQS) in 2002, J. Geophys. Res.-Atmos., 108, 4682, doi:10.1029/2003JD003863, 2003.

DeCarlo, P. F., Kimmel, J. R., Trimborn, A., Northway, M. J., Jayne, J. T., Aiken, A. C., Gonin, M., Fuhrer, K., Horvath, T., Docherty, K. S., Worsnop, D. R., and Jimenez, J. L.: Field-deployable, high-resolution, time-of-flight aerosol mass spectrometer, Anal. Chem., 78, 8281–8289, 2006.

Donahue, N. M., Robinson, A. L., Stanier, C. O., and Pandis, S. N.: Coupled partitioning, dilution, and chemical aging of semivolatile organics, Environ. Sci. Technol., 40, 2635–2643, 2006.

Donahue, N. M., Epstein, S. A., Pandis, S. N., and Robinson, A. L.: A two-dimensional volatility basis set: 1. organic-aerosol mixing thermodynamics, Atmos. Chem. Phys., 11, 3303—3318, doi:10.5194/acp-11-3303-2011, 2011.

Donahue, N. M., Henry, K. M., Mentel, T. F., Kiendler-Scharr, A., Spindler, C., Bohn, B., Brauers, T., Dorn, H. P., Fuchs, H., Tillmann, R., Wahner, A., Saathoff, H., Naumann, K. H., Mohler, O., Leisner, T., Muller, L., Reinnig, M. C., Hoffmann, T., Salo, K., Hallquist, M., Frosch, M., Bilde, M., Tritscher, T., Barmet, P., Praplan, A. P., DeCarlo, P. F., Dommen, J., Prevot, A. S. H., and Baltensperger, U.: Aging of biogenic secondary organic aerosol via gas-phase OH radical reactions, Proc. Natl. Acad. Sci. USA, 109, 13503–13508, 2012.

El Haddad, I., D'Anna, B., Temime-Roussel, B., Nicolas, M., Boreave, A., Favez, O., Voisin, D., Sciare, J., George, C., Jaffrezo, J.-L., Wortham, H., and Marchand, N.: Towards a better understanding of the origins, chemical composition and aging of oxygenated organic aerosols: case study of a Mediterranean industrialized environment, Marseille, Atmos. Chem. Phys., 13, 7875–7894, doi:10.5194/acp-13-7875-2013, 2013.

Elsasser, M., Crippa, M., Orasche, J., DeCarlo, P. F., Oster, M., Pitz, M., Cyrys, J., Gustafson, T. L., Pettersson, J. B. C., Schnelle-Kreis, J., Prévôt, A. S. H., and Zimmermann, R.: Organic molecular markers and signature from wood combustion particles in winter ambient aerosols: aerosol mass spectrometer (AMS) and high time-resolved GC-MS measurements in Augsburg, Germany, Atmos. Chem. Phys., 12, 6113–6128, doi:10.5194/acp-12-6113-2012, 2012.

Favez, O., El Haddad, I., Piot, C., Boréave, A., Abidi, E., Marchand, N., Jaffrezo, J.-L., Besombes, J.-L., Personnaz, M.-B., Sciare, J., Wortham, H., George, C., and D'Anna, B.: Inter-comparison of source apportionment models for the estimation of wood burning

aerosols during wintertime in an Alpine city (Grenoble, France), Atmos. Chem. Phys., 10, 5295–5314, doi:10.5194/acp-10-5295-2010, 2010.

Freutel, F., Schneider, J., Drewnick, F., von der Weiden-Reinmüller, S.-L., Crippa, M., Prévôt, A. S. H., Baltensperger, U., Poulain, L., Wiedensohler, A., Sciare, J., Sarda-Estève, R., Burkhart, J. F., Eckhardt, S., Stohl, A., Gros, V., Colomb, A., Michoud, V., Doussin, J. F., Borbon, A., Haeffelin, M., Morille, Y., Beekmann, M., and Borrmann, S.: Aerosol particle measurements at three stationary sites in the megacity of Paris during summer 2009: meteorology and air mass origin dominate aerosol particle composition and size distribution, Atmos. Chem. Phys., 13, 933–959, doi:10.5194/acp-13-933-2013, 2013.

Grieshop, A. P., Logue, J. M., Donahue, N. M., and Robinson, A. L.: Laboratory investigation of photochemical oxidation of organic aerosol from wood fires 1: measurement and simulation of organic aerosol evolution, Atmos. Chem. Phys., 9, 1263–1277, doi:10.5194/acp-9-1263-2009, 2009.

Hallquist, M., Wenger, J. C., Baltensperger, U., Rudich, Y., Simpson, D., Claeys, M., Dommen, J., Donahue, N. M., George, C., Goldstein, A. H., Hamilton, J. F., Herrmann, H., Hoffmann, T., Iinuma, Y., Jang, M., Jenkin, M. E., Jimenez, J. L., Kiendler-Scharr, A., Maenhaut, W., McFiggans, G., Mentel, Th. F., Monod, A., Prévôt, A. S. H., Seinfeld, J. H., Surratt, J. D., Szmigielski, R., and Wildt, J.: The formation, properties and impact of secondary organic aerosol: current and emerging issues, Atmos. Chem. Phys., 9, 5155–5236, doi:10.5194/acp-9-5155-2009, 2009.

He, L.-Y., Lin, Y., Huang, X.-F., Guo, S., Xue, L., Su, Q., Hu, M., Luan, S.-J., and Zhang, Y.-H.: Characterization of high-resolution aerosol mass spectra of primary organic aerosol emissions from Chinese cooking and biomass burning, Atmos. Chem. Phys., 10, 11535–11543, doi:10.5194/acp-10-11535-2010, 2010.

Healy, R. M., Sciare, J., Poulain, L., Kamili, K., Merkel, M., Müller, T., Wiedensohler, A., Eckhardt, S., Stohl, A., Sarda-Estève, R., McGillicuddy, E., O'Connor, I. P., Sodeau, J. R., and Wenger, J. C.: Sources and mixing state of size-resolved elemental carbon particles in a European megacity: Paris, Atmos. Chem. Phys., 12, 1681–1700, doi:10.5194/acp-12-1681-2012, 2012.

Heringa, M. F., DeCarlo, P. F., Chirico, R., Tritscher, T., Dommen, J., Weingartner, E., Richter, R., Wehrle, G., Prévôt, A. S. H., and Baltensperger, U.: Investigations of primary and secondary particulate matter of different wood combustion appliances with a high-resolution time-of-flight aerosol mass spectrometer, Atmos. Chem. Phys., 11, 5945–5957, doi:10.5194/acp-11-5945-2011, 2011.

Heringa, M. F., DeCarlo, P. F., Chirico, R., Tritscher, T., Clairotte, M., Mohr, C., Crippa, M., Slowik, J. G., Pfaffenberger, L., Dommen, J., Weingartner, E., Prévôt, A. S. H., and Baltensperger, U.: A new method to discriminate secondary organic aerosols from different sources using high-resolution aerosol mass spectra, Atmos. Chem. Phys., 12, 2189–2203, doi:10.5194/acp-12-2189-2012, 2012.

Holzinger, R., Warneke, C., Hansel, A., Jordan, A., Lindinger, W., Scharffe, D. H., Schade, G., and Crutzen, P. J.: Biomass burning as a source of formaldehyde, acetaldehyde, methanol, acetone, acetonitrile, and hydrogen cyanide, Geophys. Res. Lett., 26, 1161–1164, 1999.

Holzinger, R., Williams, J., Salisbury, G., Klüpfel, T., de Reus, M., Traub, M., Crutzen, P. J., and Lelieveld, J.: Oxygenated compounds in aged biomass burning plumes over the Eastern Mediterranean: evidence for strong secondary production of methanol and acetone, Atmos. Chem. Phys., 5, 39–46, doi:10.5194/acp-5-39-2005, 2005.

Jimenez, J. L., Canagaratna, M. R., Donahue, N. M., Prevot, A. S. H., Zhang, Q., Kroll, J. H., DeCarlo, P. F., Allan, J. D., Coe, H., Ng, N. L., Aiken, A. C., Docherty, K. S., Ulbrich, I. M., Grieshop, A. P., Robinson, A. L., Duplissy, J., Smith, J. D., Wilson, K. R., Lanz, V. A., Hueglin, C., Sun, Y. L., Tian, J., Laaksonen, A., Raatikainen, T., Rautiainen, J., Vaattovaara, P., Ehn, M., Kulmala, M., Tomlinson, J. M., Collins, D. R., Cubison, M. J., Dunlea, E. J., Huffman, J. A., Onasch, T. B., Alfarra, M. R., Williams, P. I., Bower, K., Kondo, Y., Schneider, J., Drewnick, F., Borrmann, S., Weimer, S., Demerjian, K., Salcedo, D., Cottrell, L., Griffin, R., Takami, A., Miyoshi, T., Hatakeyama, S., Shimono, A., Sun, J. Y., Zhang, Y. M., Dzepina, K., Kimmel, J. R., Sueper, D., Jayne, J. T., Herndon, S. C., Trimborn, A. M., Williams, L. R., Wood, E. C., Middlebrook, A. M., Kolb, C. E., Baltensperger, U., and Worsnop, D. R.: Evolution of organic aerosols in the atmosphere, Science, 326, 1525–1529, 2009.

Jordan, C., Fitz, E., Hagan, T., Sive, B., Frinak, E., Haase, K., Cottrell, L., Buckley, S., and Talbot, R.: Long-term study of VOCs measured with PTR-MS at a rural site in New Hampshire with urban influences, Atmos. Chem. Phys., 9, 4677–4697, doi:10.5194/acp-9-4677-2009, 2009.

Karl, T. G., Christian, T. J., Yokelson, R. J., Artaxo, P., Hao, W. M., and Guenther, A.: The Tropical Forest and Fire Emissions Experiment: method evaluation of volatile organic compound emissions measured by PTR-MS, FTIR, and GC from tropical biomass burning, Atmos. Chem. Phys., 7, 5883–5897, doi:10.5194/acp-7-5883-2007, 2007.

Kroll, J. H., Smith, J. D., Che, D. L., Kessler, S. H., Worsnop, D. R., and Wilson, K. R.: Measurement of fragmentation and functionalization pathways in the heterogeneous oxidation of oxidized organic aerosol, Phys. Chem. Chem. Phys., 11, 8005–8014, 2009.

Lanz, V. A., Alfarra, M. R., Baltensperger, U., Buchmann, B., Hueglin, C., and Prévôt, A. S. H.: Source apportionment of submicron organic aerosols at an urban site by factor analytical modelling of aerosol mass spectra, Atmos. Chem. Phys., 7, 1503–1522, doi:10.5194/acp-7-1503-2007, 2007.

Lanz, V. A., Prévôt, A. S. H., Alfarra, M. R., Weimer, S., Mohr, C., DeCarlo, P. F., Gianini, M. F. D., Hueglin, C., Schneider, J., Favez, O., D'Anna, B., George, C., and Baltensperger, U.: Characterization of aerosol chemical composition with aerosol mass spectrometry in Central Europe: an overview, Atmos. Chem. Phys., 10, 10453–10471, doi:10.5194/acp-10-10453-2010, 2010.

Lindinger, W., Hansel, A., and Jordan, A.: Proton-transfer-reaction mass spectrometry (PTR-MS): on-line monitoring of volatile organic compounds at pptv levels, Chem. Soc. Rev., 27, 347–354, 1998.

Mohr, C., DeCarlo, P. F., Heringa, M. F., Chirico, R., Slowik, J. G., Richter, R., Reche, C., Alastuey, A., Querol, X., Seco, R., Peñuelas, J., Jiménez, J. L., Crippa, M., Zimmermann, R., Baltensperger, U., and Prévôt, A. S. H.: Identification and quantification of organic aerosol from cooking and other sources in Barcelona using aerosol mass spectrometer data, Atmos. Chem. Phys., 12, 1649–1665, doi:10.5194/acp-12-1649-2012, 2012.

Ng, N. L., Canagaratna, M. R., Zhang, Q., Jimenez, J. L., Tian, J., Ulbrich, I. M., Kroll, J. H., Docherty, K. S., Chhabra, P. S., Bahreini, R., Murphy, S. M., Seinfeld, J. H., Hildebrandt, L., Donahue, N. M., DeCarlo, P. F., Lanz, V. A., Prévôt, A. S. H., Dinar, E., Rudich, Y., and Worsnop, D. R.: Organic aerosol components observed in Northern Hemispheric datasets from Aerosol Mass Spectrometry, Atmos. Chem. Phys., 10, 4625–4641, doi:10.5194/acp-10-4625-2010, 2010.

Paatero, P.: The multilinear engine - A table-driven, least squares program for solving multilinear problems, including the n-way parallel factor analysis model, J. Comput. Graph. Stat., 8, 854–888, 1999.

Paatero, P. and Hopke, P. K.: Discarding or downweighting high-noise variables in factor analytic models, Anal. Chim. Acta, 490, 277–289, 2003.

Paatero, P. and Tapper, U.: Positive matrix factorization – a nonnegative factor model with optimal utilization of error-estimates of data values, Environmetrics, 5, 111–126, 1994.

Piot, C., Jaffrezo, J.-L., Cozic, J., Pissot, N., El Haddad, I., Marchand, N., and Besombes, J.-L.: Quantification of levoglucosan and its isomers by High Performance Liquid Chromatography – Electrospray Ionization tandem Mass Spectrometry and its applications to atmospheric and soil samples, Atmos. Meas. Tech., 5, 141–148, doi:10.5194/amt-5-141-2012, 2012.

Robinson, A. L., Donahue, N. M., Shrivastava, M. K., Weitkamp, E. A., Sage, A. M., Grieshop, A. P., Lane, T. E., Pierce, J. R., and Pandis, S. N.: Rethinking organic aerosols: Semivolatile emissions and photochemical aging, Science, 315, 1259–1262, 2007.

Sandradewi, J., Prevot, A. S. H., Szidat, S., Perron, N., Alfarra, M. R., Lanz, V. A., Weingartner, E., and Baltensperger, U.: Using aerosol light absorption measurements for the quantitative determination of wood burning and traffic emission contributions to particulate matter, Environ. Sci. Technol., 42, 3316–3323, 2008.

Schauer, J. J., Kleeman, M. J., Cass, G. R., and Simoneit, B. R. T.: Measurement of emissions from air pollution sources. 3. C-1-C-29 organic compounds from fireplace combustion of wood, Environ. Sci. Technol., 35, 1716–1728, 2001.

Schauer, J. J., Kleeman, M. J., Cass, G. R., and Simoneit, B. R. T.: Measurement of emissions from air pollution sources. 4. C-1-C-27 organic compounds from cooking with seed oils, Environ. Sci. Technol., 36, 567–575, 2002.

Sciare, J., D'Argouges, O., Estève, R. S., Gaimoz, C., Dolgorouky, C., Bonnaire, N., Favez, O., Bonsang, B., and Gros, V.: Large contribution of water insoluble secondary organic aerosols in the region of Paris (France) during wintertime, J. Geophys. Res., 116, D22203, doi:10.1029/2011JD015756, 2011.

Simoneit, B. R. T., Schauer, J. J., Nolte, C. G., Oros, D. R., Elias, V. O., Fraser, M. P., Rogge, W. F., and Cass, G. R.: Levoglucosan, a tracer for cellulose in biomass burning and atmospheric particles, Atmos. Environ., 33, 173-182, 1999.

Slowik, J. G., Vlasenko, A., McGuire, M., Evans, G. J., and Abbatt, J. P. D.: Simultaneous factor analysis of organic particle and gas mass spectra: AMS and PTR-MS measurements at an urban site, Atmos. Chem. Phys., 10, 1969–1988, doi:10.5194/acp-10-1969-2010, 2010.

Sun, Y. L., Zhang, Q., Schwab, J. J., Yang, T., Ng, N. L., and Demerjian, K. L.: Factor analysis of combined organic and inorganic aerosol mass spectra from high resolution aerosol mass spectrometer measurements, Atmos. Chem. Phys., 12, 8537–8551, doi:10.5194/acp-12-8537-2012, 2012.

Talbot, R., Mao, H. T., and Sive, B.: Diurnal characteristics of surface level O_3 and other important trace gases in New England, J. Geophys. Res.-Atmos., 110, D09307, doi:10.1029/2004JD005449, 2005.

Ulbrich, I. M., Canagaratna, M. R., Zhang, Q., Worsnop, D. R., and Jimenez, J. L.: Interpretation of organic components from Positive Matrix Factorization of aerosol mass spectrometric data, Atmos. Chem. Phys., 9, 2891–2918, doi:10.5194/acp-9-2891-2009, 2009.

Vlasenko, A., Slowik, J. G., Bottenheim, J. W., Brickell, P. C., Chang, R. Y. W., Macdonald, A. M., Shantz, N. C., Sjostedt, S. J., Wiebe, H. A., Leaitch, W. R., and Abbatt, J. P. D.: Measurements of VOCs by proton transfer reaction mass spectrometry at a rural Ontario site: Sources and correlation to aerosol composition, J. Geophys. Res.-Atmos., 114, D21305, doi:10.1029/2009JD012025, 2009.

Vlasenko, A., Macdonald, A .M., Sjostedt, S. J., and Abbatt, J. P. D.: Formaldehyde measurements by Proton transfer reaction – Mass Spectrometry (PTR-MS): correction for humidity effects, Atmos. Meas. Tech., 3, 1055–1062, doi:10.5194/amt-3-1055-2010, 2010.

Warneke, C., de Gouw, J. A., Goldan, P. D., Kuster, W. C., Williams, E. J., Lerner, B. M., Jakoubek, R., Brown, S. S., Stark, H., Aldener, M., Ravishankara, A. R., Roberts, J. M., Marchewka, M., Bertman, S., Sueper, D. T., McKeen, S. A., Meagher, J. F., and Fehsenfeld, F. C.: Comparison of daytime and nighttime oxidation of biogenic and anthropogenic VOCs along the New England coast in summer during New England Air Quality Study 2002, J. Geophys. Res.-Atmos., 109, D10309, doi:10.1029/2003JD004424, 2004.

Yuan, B., Shao, M., de Gouw, J., Parrish, D. D., Lu, S., Wang, M., Zeng, L., Zhang, Q., Song, Y., Zhang, J., and Hu, M.: Volatile organic compounds (VOCs) in urban air: How chemistry affects the interpretation of positive matrix factorization (PMF) analysis, J. Geophys. Res.-Atmos., 117, D24302, doi:10.1029/2012JD018236, 2012.

Zhang, Q., Jimenez, J. L., Canagaratna, M. R., Allan, J. D., Coe, H., Ulbrich, I., Alfarra, M. R., Takami, A., Middlebrook, A. M., Sun, Y. L., Dzepina, K., Dunlea, E., Docherty, K., DeCarlo, P. F., Salcedo, D., Onasch, T., Jayne, J. T., Miyoshi, T., Shimono, A., Hatakeyama, S., Takegawa, N., Kondo, Y., Schneider, J., Drewnick, F., Borrmann, S., Weimer, S., Demerjian, K., Williams, P., Bower, K., Bahreini, R., Cottrell, L., Griffin, R. J., Rautiainen, J., Sun, J. Y., Zhang, Y. M., and Worsnop, D. R.: Ubiquity and dominance of oxygenated species in organic aerosols in anthropogenically-influenced Northern Hemisphere midlatitudes, Geophys. Res. Lett., 34, L13801, doi:10.1029/2007GL029979, 2007.

Zhang, Q., Jimenez, J., Canagaratna, M., Ulbrich, I., Ng, N., Worsnop, D., and Sun, Y.: Understanding atmospheric organic aerosols via factor analysis of aerosol mass spectrometry: a review, Anal. Bioanal. Chem., 401, 3045–3067, 2011.